Cortical Mapping by Magnetic Resonance Imaging (MRI) and Quantitative Cytological Analysis in the Human Brain: A Feasibility Study in the Fusiform Gyrus

Natalie M. Schenker-Ahmed and **Jacopo Annese**[*]

The Brain Observatory, San Diego and Department of Radiology, University of California, San Diego

Abstract

The cerebral cortex is a layered cellular structure that is tangentially organized into a mosaic of anatomically and functionally distinct fields. In spite of centuries of investigation, the precise localization and classification of many areas in the cerebral cortex remain problematic because the relationship between functional specificity and intra-cortical structure has not been firmly established. Furthermore, it is not yet clear how surface landmarks, visible through gross examination and, more recently, using non-invasive magnetic resonance imaging (MRI), relate to underlying microstructural borders and to the topography of functional activation.

We have designed a multi-modal neuroimaging protocol that combines MRI and quantitative microscopic analysis in the same individual to clarify the topography of cytoarchitecture underlying gross anatomical landmarks in the cerebral cortex. We tested our approach in the region of the fusiform gyrus (FG), because in spite of its seemingly smooth appearance on the ventral aspect of both hemispheres, this structure houses many functionally defined areas whose histological borders remain unclear. In practice, we used MRI-based automated segmentation to define the region of interest from which we could then collect quantitative histological data (specifically, neuronal size and density). A modified stereological approach was used to sample the cortex within the FG without *a priori* assumptions on the location of architectonic boundaries. The results of these analyses illustrate architectonic variations along the FG and demonstrate that it is possible to correlate quantitative histological data to measures that are obtained in the context of large-scale, non-invasive MRI-based population studies.

Keywords

1. Introduction

Cortical areas (Barbas et al., 2002; Annese et al., 2005) can be functionally and anatomically defined according to several established criteria (van Essen and Maunsell, 1980; Kaas, 2010). In most circumstances, direct physiological recording of the human cerebral cortex is precluded by obvious practical and ethical concerns; nevertheless, functional subdivisions

[*]Corresponding Author: Jacopo Annese PhD, The Brain Observatory, 3510 Dunhill St., San Diego, CA 92122, jannese@ucsd.edu, tel: (858)822-4465, fax: (858)534-6046.

can be localized non-invasively through the use of functional magnetic resonance imaging (fMRI; Devlin et al., 2006) or positron emission tomography (PET; Haxby et al., 1994). Traditionally, the anatomical boundaries between functionally defined cortical areas could only be verified through studies of architectonics and connectivity patterns (Kaas, 2010) that were conducted on postmortem tissue and in experimental animals. The need to link MRI localization of functional landmarks to maps based on underlying microstructuralanatomy has been previously raised multiple times (Crick and Jones, 1993; Passingham et al., 2002; Devlin and Poldrack, 2007). Toward this end, advances in the use of high-resolution MR to identify cortical boundaries have enabled researchers to localize regions with prominent features such as the stria of Gennari (Clark et al., 1992; Bridge et al., 2005) and the boundary between motor and somatosensory cortex (Glasser and van Essen, 2011). As evidenced by direct comparisons with histology, these borders are likely visible in MRI scans because of variations in the density of myelinated fibers (Geyer et al., 2011a, 2011b). However, histological studies and brain mapping using MRI are rarely conducted on the same subjects (Annese, 2012); thus, the relationship between MRI data and microanatomical structure as seen in histological examination remains unclear.

For example, the fusiform gyrus (FG) is an anatomical structure on the ventral surface of the cerebrum that is long and uninterrupted in appearance except for very shallow secondary sulci. While there are no gross anatomical landmarks that could be used to subdivide the FG into separate compartments, the gyrus houses several distinct regions involved in diverse cognitive functions, such as face recognition (Natu and O'Toole, 2011; Meng et al., 2012), orthography and reading (Devlin et al., 2006; Tsapkini and Rapp, 2010), semantic word retrieval (Perani et al., 1999; Sharp et al., 2010), processing of color information (Martin et al., 1995; Simmons et al., 2007), synesthesia (Jäncke et al., 2009) and other functions related to object identification (Wierenga et al., 2009). Linking the function of the FG to underlying micro-anatomical parcels is problematic, because there are too few published histological reports and images that can be related to the variety of functions observed *in vivo*. Classical maps of the cerebral cortex, constructed on meticulous, but subjective, observations on the size and distribution of neuronal cell bodies (Brodmann, 1909; von Economo, 1929) or the density and arrangement of myelinated fibers (Vogt and Vogt, 1919; Hopf, 1951), subdivide the FG into only two or three sub-regions (Figure 1). The lack of clear quantitative criteria and documentation makes it difficult to reference these studies when mapping the cortex of any individual subject.

In an effort to address these limitations in the field, we propose a novel method that can help establish a more direct correlation between quantitative cyto-architectonic data and MRI-based maps in the human brain. The proposed method leverages the combination of non-invasive MRI and postmortem imaging of the brain in the same individual at different levels of resolution. MRI is used to determine, via established segmentation algorithms, a region of interest (ROI) that is unique and reproducible across larger, population based, neuroimaging studies. In this study, we applied the FreeSurfer image processing pipeline (http://surfer.nmr.mgh.harvard.edu/; Fischl et al., 2004; Desikan et al., 2006) to label voxels that belong to the FG. These voxels are represented by corresponding vertices in the triangulated model of the surface of the cerebral cortex. Once the ROI was selected, we applied stereological tools to acquire quantitative data from whole-brain histological sections that cross the ROI. This approach allows for the analysis of stereological quantitative data, created without the bias of *a priori* assumptions regarding the location of architectonic boundaries within the FG; crucially, information describing microarchitecture can be related to other maps obtained with MRI and fMRI via the standard FreeSurfer segmentation. By combining these two robust approaches (automated segmentation and stereology), we demonstrate the potential to bridge the gap between two levels of mapping at the macro- and

microscopic level and produce quantitative data in a way that directly relates to MRI features that are relevant to clinical and morphological population-based studies.

2. Materials and methods

2.1. The brain

This feasibility study was conducted using a single brain specimen, donated by a 50-year old Hispanic male. The subject was a smoker (for 30 years), and had received cataract surgery in both eyes 6 months prior to his death. The donor worked as a private investigator.

2.2. Magnetic resonance imaging (MRI)

MRI scans of the brain were acquired *in situ* on an General Electric "HDX" Twinspeed EXCITE 1.5T scanner (Milwaukee, WI.) using an eight-channel, transmit-receive, phased-array head coil. Scan parameters (3-D acquisition, T1-weighted, fast gradient echo; pixel spacing: 0.9375mm × 0.9375mm; slice thickness: 1.2mm; TE=4.832; TR=10.612) were selected to allow robust reconstruction of the brain's cortical surface and automated segmentation of the cortex using FreeSurfer (Fischl et al., 2004; Desikan et al., 2006).

2.3. Histology

After extraction, the specimen was fixed in 4% paraformaldehyde for 10 weeks and then cryoprotected in a series of buffered phosphate solutions with increasing concentrations of sucrose up to 30%. The whole brain was embedded in a gelatin-sucrose matrix and oriented so that the coronal plane was orthogonal to the AC-PC line (Talairach and Tournoux, 1988). The brain-gelatin block was frozen in isopentane at -40°C and sectioned whole in the coronal plane at an interval of 70μm on a modified sliding microtome (based on a Leica SM2500, Leica Microsystems, Inc., Buffalo Grove, IL). Before each section was cut (2,251 sections were collected in total), a photograph of the blockface was acquired using a digital camera mounted directly above the microtome stage (Nikon D700 – AF NIKKOR 35mm f/ 2D lens; Nikon Inc., Melville, NY). The resolution of the blockface images was 45μm/pixel (Figure 2A). Every section was stored in a buffered phosphate solution (pH 7.4). To generate a complete series through the brain, 1 in 36 sections was mounted on large format glass slides (5 in. × 7 in.) and stained for cell bodies using thionin dye (Nissl staining; Fig. 2B; Simmons and Swanson, 1993).

2.4. Region of Interest Definition

A surface reconstruction and cortical parcellation were created from the MRI scan using FreeSurfer; the basics of automated parcellation have been described in detail elsewhere (Dale et al., 1999; Fischl et al., 2004; Desikan et al., 2006). Surfaces were generated automatically after intensity correction. The pial surface generated from FreeSurfer and the original MRI were loaded into Amira (VSG, Visualization Science Group, Inc., Burlington MA) and visualized concurrently. The pial surface reconstruction and the MRI data were co-registered in order to observe the extent of the FG as it appears in the coronal sections of the MRI data. The boundaries of the FG as defined by the FreeSurfer parcellation were then manually delineated on the corresponding images of the blockface (Figure 3).

2.5. Stereology

Using the delineated blockface images as a reference, the boundaries of the FG were manually traced as contours with Stereo Investigator (MicroBrightfield, Williston, VT). To estimate total neuron numbers within the FG, we examined every Nissl-stained section containing the ROI (31 sections in the left hemisphere and 30 sections in the right hemisphere). For each section, we acquired image stacks through the depth of the cortex

using a 60×/1.42 N.A. oil immersion lens in a systematic randomly sampled $1000 \times 1000\mu m$ grid (Figure 4B). Each image stack comprised 25 images separated by $1\mu m$ distance in the z-axis.

The data files and image stacks were loaded into Stereo Investigator on a Dell XPS 730x for analysis. For the analysis of the virtual stacks in each section, we used the optical fractionator method (West et al., 1991) with a 50×50-μm counting frame. We used a standard dissector depth of $10\mu m$ with a $2\mu m$ guard zone. Section thickness was measured at each probe site. Neurons were counted only if a clear nucleolus came into focus within the permitted boundaries of the counting frame, according to the principles of the optical fractionator method (Figure 4A; West et al., 1991). The perikaryal volume of each counted neuron was measured using the nucleator probe (Gundersen et al., 1988). The data were acquired by two raters with a high inter-rater reliability (Pearson's $r = 0.98$).

2.6. Selection of subregions of interest (for post-hoc analysis)

We digitized each Nissl-stained slide using an ultra-high resolution flat bed scanner (Creo Eversmart Supreme II; Eastman Kodak Company, Rochester, NY) at a resolution of 4880 dpi. (The resulting images are approximately equivalent to images acquired through a microscope with a 2x objective). The six cortical layers were identified within the ROI in each section and divided into supragranular (layers II and III) and infragranular (layers V and VI) regions. This categorization was used to divide the data into separate groups for independent post-hoc analysis.

In addition, an adjacent series of 1 in 36 sections was stained for myelinated fibers using a modification of the Gallyas silver impregnation protocol (Figure 2C; Gallyas, 1979), and, using previously described methods (Annese et al., 2004), potential myelo-architectonic sub-regions of the FG were identified to use as additional criteria for post-hoc analysis.

2.7. Statistics

The data from supragranular and infragranular sub regions were separated for independent analysis. These data were further divided into four smaller samples based on the four identified myelo-architectonic sub-regions for additional analysis. Within each sub region, cell number and density as well as average perikaryal volume were estimated. The effects of subregion, hemisphere, and layer (infragranular vs. supragranular) on the data were assessed using the R statistics package (R-Development, 2009) to run ANOVA analyses. An asymmetry coefficient for each variable and region was calculated using the equation (R – L)/[(R + L)/2].

3. Results

3.1. Volume measurements

The total volume of the FG was 8252 mm^3 in the right hemisphere and 7936 mm^3 in the left hemisphere. In both hemispheres, the most posterior sub-region occupied the least territory (Region D, 660 mm^3, right; 564 mm^3, left). The largest sub-region in the right hemisphere was more anterior (Region B, 3962 mm^3) than the largest in the left hemisphere (Region C, 2816 mm3; Table I).

3.2. Neuron size

The perikaryal volume of counted neurons ranged from near 400 μm^3 in the posterior regions to more than 1100 μm^3 in the anterior regions (Table II; Figure 5A,5B). All variables had significant effects on average perikaryal volume (Region, $F_{3,3}=72.39$, p=0.0004; layer, $F_{1,3}=32.07$, p=0.0002; and hemisphere, $F_{1,3}=7.60$, p=0.02), with no

significant interactions among variables. The range in average perikaryal volume displayed a reverse correlation to estimated neuronal densities (r=-0.879).

3.3. Neuronal number and density

The estimated numbers of neurons can be found in Table II. Coefficients of error were 0.05 (Gundersen, m=1) for all measures. Region ($F_{3,3}$=603.43, p=0.0001), layer ($F_{1,3}$=50.56, p=0.006), and hemisphere ($F_{1,3}$=69.23, p=0.004) all had significant effects on neuronal density, but no interactions were observed among variables. All sub-regions were significantly different from each other, with more anterior regions having less neuronal density than regions more posteriorly located (Figure 5C,5D). The left FG displayed greater neuronal density than the right FG; and overall density was greater in supragranular layers than in infragranular layers.

3.4. Asymmetry

Analyses showed an asymmetry in neuronal density, with the left FG having a greater density in most regions than the right FG (Table III). A reverse relationship was seen in average perikaryal volume, with the neurons being larger overall in the right FG than in the left FG. In general, the volume of the entire gyrus showed no marked asymmetry.

4. Discussion

We evaluated a novel method to help clarify the relationship between macroscopic sulcal landmarks detectable with MRI and anatomical microstructure within the FG. In humans, the knowledge gap between these two aspects of neural structure and their relationship to the topography of functional specificity remains significant because direct physiological recording is not easily afforded (Ojemann et al., 1989; Vidorreta et al., 2011; Parvizi et al., 2012). It is important to address the issue from an ontological perspective first because if microstructural data are to inform brainmapping studies at large, these data must be produced and reported in the wider neuroimaging context and not limited to the few specimens that are analyzed postmortem. Hundreds of MRI studies utilize FreeSurfer's segmentation scheme as a reference to define ROIs and to report the anatomical correlates of their morphological phenomena or functional activation (Fischl, 2012). Therefore, we adopted the output of the FreeSurfer-based anatomical segmentation applied to the MRI scan of the brain to define our ROI, in this case the FG. The main advantage of using automated MRI-based parcellation schemes lies in the added consistency and reproducibility of definitions and final results of analyses. Following the standard delineation of the ROI, we used stereology as the foundation for our data acquisition model. Although many studies have adopted the term 'stereology' to imply an observer-independent approach to cortical architectonics (Schleicher et al., 2000), stereology, strictly speaking, refers to very well-defined unbiased sampling strategies to quantify measurable features in a 3-D structure based on 2-D cross sections (Gundersen and Jensen, 1987). Standard stereological protocols require the sampling of 10-15 sections across each ROI and, for the optical fractionator in particular, it is necessary to define the sampling grid (in microns) so that a count of approximately 200 neurons can be obtained within each ROI. Our goal was to investigate the cyto-architectonic landscape within the MRI-based FG ROI, without imposing *a priori* structural borders for the analysis, but rather reporting the emergence of transitions in terms of cytological parameters (i.e., neuronal size and density). This approach required increasing the number of sections sampled through the FG as well as increasing the number of sampling points on each histological section (i.e., smaller sampling grid).

Although based on a single specimen, the quantitative data obtained in the context of our feasibility study reveals interesting patterns at the microscopic level that can be related to

the map of cognitive functions within the FG. Classic studies suggest that the FG is not an anatomically uniform structure, (Brodmann, 1909; von Economo, 1929), and recent cyto-architectonic studies have identified multiple subdivisions within this gyrus (Caspers et al., 2012). We have also analyzed myelination patterns (Annese et al., 2004) in our ROI (Figure 6) and observed transitions and architectures analogous to those reported by Hopf (1951). Stereological data (neuronal density and perikaryal volume) show a trend towards smaller neurons and higher neuronal density in posterior FG relative to the anterior FG. This effect is interesting in the light of what we know about functional maps in FG. Posterior regions are activated in facial processing (Natu and O'Toole, 2011; Meng et al., 2012), orthographic processing (Tsapkini and Rapp, 2010), and other types of detail oriented data processing (Price et al., 2003), and are located relatively downstream in the ventral visual processing stream. More anterior regions perform more abstract and integrative processing, likely incorporating inputs across multiple modalities and cortical areas (Price et al., 2003). Previously published studies also suggest that 'big picture' processing occurs in the right FG while more 'detail oriented' processing is mapped in the left (Meng et al., 2012). Interestingly, when we analyzed our results to study the asymmetry between hemispheres, the left FG exhibited an overall greater neuronal density and smaller neuron volume compared to the right.

Thus, we find that in regions that are thought to involve processing of features at the local level, the neurons tend to be smaller and more tightly packed. In contrast, in areas where greater integration of information is required, the neurons are larger and more widely spaced. This observation suggests a correlation between neuron size and type of processing (Elston and Rockland, 2002). Larger neurons may have greater potential to receive and integrate diverse input, because of a possible association between the larger neuronal soma and longer and increased numbers of dendritic processes (Hayes and Lewis, 1996; Jacobs et al., 2001). Within this context, it may be important to mention that other regions of cortex, particularly those involved with language processing, also exhibit asymmetry in cyto-architectural features (e.g. temporal language areas, Hutsler, 2003; Broca's area, Hayes and Lewis 1996; Schenker et al., 2008). These correlations are extremely interesting and additional studies utilizing the protocol described in this communication will be required to further explore the above-mentioned hypotheses.

5. Conclusion

We present a new approach to quantitative histological analysis that relates directly to MR parcellation schemes that are widely adopted by the neuroimaging community. This approach allows us to directly relate clinically-relevant MRI data to data obtained postmortem from histological sections belonging to the same subject. The compiled data enable us to gain a better understanding of the anatomical microstructure underlying imaging data.

Stereological tools are widely used for the investigation of histological features because they provide statistically valid estimates without the need for a complete survey of the tissue. In fact, the goal is to reduce the number of sample sections and locations within each slice. This approach was necessary when the analyses were performed manually, but with computer-controlled microscopy it is possible to sample large areas and automatically acquire a large number of stacks. Leveraging the availability of modern computational power and ample digital storage, we adopted a modification of the traditional stereological approach, which effectively over-samples the ROI. This over-sampling was necessary because we did not define discrete subregions within the FG prior to obtaining the stereological data. Instead, after acquisition of stereological image stacks, we queried the data to evaluate arbitrary criteria of cortical parcellation, including myelo-architectonics.

This is only one example of the type of post hoc analyses that could be performed using the stereological data acquired from the FG (or other, larger cortical regions) in the manner that we described. Other equally valid criteria for the retrospective analysis of the raw, 'blanket'-type stereological sampling that we propose could be based on complementary histological stains (such as local variations in immunohistochemical staining), gross anatomical features (using sulcal anatomy to define borders of subregions) or functional landmarks (Kanwisher et al., 1997). Anatomical features and functional landmarks can be aligned to the histological slices via the MRI scan of the same subject, as described above.

The unbiased stereological based wide-sampling that we applied in this study allows for increased flexibility in the post-acquisition analysis. One of the main differences between this protocol and previous methods that have been used to localize architectonic borders along stretches of cortex (like the grey level index, Caspers et al., 2012; Kujovic et al., 2012 or fluid automated methods, Annese, et al. 2004), is the emphasis on providing cellular-level descriptors for functional regions highlighted by neuroimaging studies rather than on parcellation *per se*. This method recognizes that functional maps are not necessarily anchored to gross anatomical landmarks that can be readily identified across individuals.

The proposed approach has the potential to provide consistent histological 'profiles' resulting from the examination of multiple specimens. These 'profiles' would be associated with neuroimaging ontologies based on automated segmentation methods, thereby offering anatomical substantiation for neuroimaging markers and functional maps obtained non-invasively. It is also conceivable that further combined MRI-histological studies, like the one we present here, will be used to train algorithms for automated segmentation and to refine parcellation schemes.

Our method relies on a very dense stereological sampling scheme, compared to classical design-based stereology. Therefore, the parameters of such large-scale sampling protocols must be defined carefully in order to maximize efficiency while preserving accuracy. We have tested the feasibility of our approach on a specific region that can be unambiguously defined by the automated parcellation of MR images. However, the protocol could be applied to the whole brain, provided adequate resources were invested in the survey, yielding data sets of unprecedented size and richness amenable to retrospective studies based on a variety of post-hoc criteria. Furthermore, the latter could be enabled for remote investigators due to the advent of new web technologies that allow for analysis of digitized virtual slices online.

Acknowledgments

References

Annese J. The importance of combining MRI and large-scale digital histology in neuroimaging studies of brain connectivity and disease. Front Neuroinform. 2012; 6:13. [PubMed: 22536182]

Annese J, Gazzaniga M, Toga A. Localization of the Human Cortical Visual Area MT Based on Computer Aided Histological Analysis. Cereb Cortex. 2005; 15:1044–53. [PubMed: 15590914]

Annese J, Pitiot A, Dinov ID, Toga A. A myelo-architectonic method for the structural classification of cortical areas. NeuroImage. 2004; 21:15–26. [PubMed: 14741638]

Barbas, H.; Ghashghaei, H.; Rempel-Clower, N.; Xiao, D. Anatomic basis of functional specialization in prefrontal cortices in primates. In: J, G., editor. Handbook of Neuropsychology. Elsevier Science B.V.: Amsterdam; 2002. p. 1-27.

Bridge H, Clare S, Jenkinson M, Jezzard P, Parker AJ, Matthews PM. Independent anatomical and functional measures of the V1/V2 boundary in human visual cortex. 2005; 5:93–102.

Brodmann, K. Vergleichende Lokalisationslehre der Grosshirnrinde in ihren Prinzipien dargestellt auf Grund des Zellenbaues. Johann Ambrosias Barth; Leipzig: 1909.

Caspers J, Zilles K, Eickhoff S, Schleicher A, Mohlberg H, Amunts K. Cytoarchitectonical analysis and probabilistic mapping of two extrastriate areas of the human posterior fusiform gyrus. Brain Struct Funct. 2013; 218(2):511–26. [PubMed: 22488096]

Clark VP, Courchesne E, Grafe M. In vivo myeloarchitectonic analysis of human striate and extrastriate cortex using magnetic resonance imaging. Cereb Cortex. 1992; 2:417–24. [PubMed: 1422094]

Crick F, Jones E. Backwardness of human neuroanatomy. Nature. 1993; 361:109. [PubMed: 8421513]

Dale AM, Fischl B, Sereno MI. Cortical Surface-Based Analysis I: Segmentation and Surface Reconstruction. NeuroImage. 1999; 9:179–94. [PubMed: 9931268]

Desikan RS, Segonne F, Fischl B, Quinn BT, Dickerson BC, Blacker D, Buckner RL, Dale AM, Maguire RP, Hyman BT, Albert MS, Killiany RJ. An automated labeling system for subdividing the human cerebral cortex on MRI scans into gyral based regions of interest. NeuroImage. 2006; 31:968–80. [PubMed: 16530430]

Devlin J, Jamison H, Gonnerman L, Matthews P. The role of the posterior fusiform gyrus in reading. J Cogn Neurosci. 2006; 18:911–22. [PubMed: 16839299]

Devlin J, Poldrack R. In praise of tedious anatomy. NeuroImage. 2007; 37:1003–41.

Elston GN, Rockland KS. The Pyramidal Cell of the Sensorimotor Cortex of the Macaque Monkey: Phenotypic Variation. Cereb Cortex. 2002; 12:1071–8. [PubMed: 12217971]

Fischl B. FreeSurfer. NeuroImage. 2012; 62:774–81. [PubMed: 22248573]

Fischl B, van der Kouwe A, Destrieux C, Halgren E, Segonne F, Salat DH, Busa E, Seidman LJ, Goldstein J, Kennedy D, Caviness VS, Makris N, Rosen B, Dale AM. Automatically parcellating the human cerebral cortex. Cereb Cortex. 2004; 14:11–22. [PubMed: 14654453]

Gallyas F. Silver staining of myelin by means of physical development. Neurol Res. 1979; 1:203–9. [PubMed: 95356]

Geyer S, Weiss M, Reimann K, Lohmann G, Turner R. Microstructural parcellation of the human cerebral cortex—from Brodmann's post-mortem map to in vivo mapping with high-field magnetic resonance imaging. Front Hum Neurosci. 2011a; 5:19. [PubMed: 21373360]

Geyer, S.; Weiss, M.; Reimann, K.; Turner, R. 7T microstructural MR mapping of the border between primary motor and somatosensory cortex in humans. 17th Annual Meeting of the Organization for Human Brain Mapping; Quebec City, QC, Canada. 2011b.

Glasser MF, van Essen DC. Mapping Human Cortical Areas in vivo Based on Myelin Content as Revealed by T1- and T2-weighted MRI. J Neurosci. 2011; 31:11597–616. [PubMed: 21832190]

Gundersen H, Bendtsen T, Korbo L, Marcussen N, Möller A, Nielsen K, Nyengaard J, Pakkenberg B, Sorensen F, Vesterby A. Some new, simple and efficient stereological methods and their use in pathological research and diagnosis. APMIS. 1988; 96:379–94. [PubMed: 3288247]

Gundersen HJ, Jensen EB. The efficiency of systematic sampling in stereology and its prediction. J Microsc. 1987; 147:229–63. [PubMed: 3430576]

Haxby J, Horwitz B, Ungerleider LG, Maisog JM, Pietrini P, Grady CL. The Functional Organization of Human Extrastriate Cortex: A PET-rCBF Study of Selective Attention to Faces and Locations. J Neurosci. 1994; 14:6336–53. [PubMed: 7965040]

Hayes T, Lewis D. Magnopyramidal neurons in the anterior motor speech region: Dendritic features and interhemispheric comparisons. Arch Neurol. 1996; 53:1277–83. [PubMed: 8970455]

Hopf A. Die Myeloarchitektonik des Isocortex temporalis beim Menschen. J Hirnforsch. 1951; 1:208–79.

Hutsler JJ. The specialized structure of human language cortex: Pyramidal cell size asymmetries within auditory and language-associated regions of the temporal lobes. Brain Lang. 2003; 86:226–42. [PubMed: 12921766]

Jacobs B, Schall M, Prather M, Kapler E, Driscoll L, Baca S, Jacobs J, Ford K, Wainwright M, Treml M. Regional Dendritic and Spine Variation in Human Cerebral Cortex: a Quantitative Golgi Study. Cereb Cortex. 2001; 11:558–71. [PubMed: 11375917]

Jäncke L, Beeli G, Eulig C, Hänggi J. The neuroanatomy of grapheme-color synesthesia. Eur J Neurosci. 2009; 29:1287–93. [PubMed: 19302164]

Kaas, J. Cortical Circuits: Consistency and Variability across Cortical Areas and Species. In: von der Malsburg, C.; Phillips, WA.; W, S., editors. Dynamic Coordination in the Brain: From Neurons to Mind. The MIT Press; Cambridge, Massachusetts: 2010. p. 25-34.

Kanwisher N, McDermott J, Chun M. The Fusiform Face Area: A Module in Human Extrastriate Cortex Specialized for the Perception of Faces. J Neurosci. 1997; 17:4302–11. [PubMed: 9151747]

Kujovic M, Zilles K, Malikovic A, Schleicher A, Mohlberg H, Rottschy C, Eickhoff S, Amunts K. Cytoarchitectonic mapping of the human dorsal extrastriate cortex. Brain Struct Funct. 2012:1–16.

Martin A, Haxby J, Lalonde F, Wiggs C, Ungerleider L. Discrete Cortical Regions Associated with Knowledge of Color and Knowledge of Action. Science. 1995; 270:102–5. [PubMed: 7569934]

Meng M, Cherian T, Singal G, Sinha P. Lateralization of face processing in the human brain. Proc R Soc Lond, Ser B: Biol Sci. 2012; 279:2052–61.

Natu V, O'Toole A. The neural processing of familiar and unfamiliar faces: A review and synopsis. Br J Psychol. 2011; 102:726–47. [PubMed: 21988381]

Ojemann G, Ojemann J, Lettich E, Berger M. Cortical language localization in left, dominant hemisphere. J Neurosurg. 1989; 71:316–26. [PubMed: 2769383]

Parvizi J, Jacques C, Foster BL, Withoft N, Rangarajan V, Weinder KS, Grill-Spector K. Electrical Stimulation of Human Fusiform Face-Selective Regions Distorts Face Perception. J Neurosci. 2012; 32:14915–20. [PubMed: 23100414]

Passingham RE, Stephan KE, Kotter R. The anatomical basis of functional localization in the cortex. Nat Rev Neurosci. 2002; 3:606–16. [PubMed: 12154362]

Perani D, Schnur T, Tettamanti M, Italy, Cappa SF, Fazio F. Word and picture matching: a PET study of semantic category effects. Neuropsychologia. 1999; 37:293–306. [PubMed: 10199643]

Price C, Noppeney U, Phillips J, Devlin J. How is the fusiform gyrus related to category-specificity? Cognit Neuropsychol. 2003; 20:561–74. [PubMed: 20957585]

R-Development CT. R: A Language and Environment for Statistical Computing. R Foundation for Statistical Computing; Vienna, Austria: 2009.

Schenker N, Buxhoeveden D, Blackmon W, Amunts K, Zilles K, Semendeferi K. A comparative quantitative analysis of cytoarchitecture and minicolumnar organization in Broca's area in humans and great apes. J Comp Neurol. 2008; 810:117–28. [PubMed: 18612968]

Schleicher A, Amunts K, Geyer S, Kowalski T, Schormann T, Palomero-Gallagher N, Zilles K. A stereological approach to human cortical architecture: identification and delineation of cortical areas. J Chem Neuroanat. 2000; 20:31–47. [PubMed: 11074342]

Sharp D, Awad M, Warren J, Wise R, Vigliocco G, Scott S. The neural response to changing semantic and perceptual complexity during language processing. Hum Brain Mapp. 2010; 31:365–77. [PubMed: 19777554]

Simmons D, Swanson L. The Nissl stain. Neurosci Prot. 1993 93-050-12-01-07.

Simmons W, Ramjee V, Baeauchamp M, McRae K, Martin A, Barsalou L. A common neural substrate for perceiving and knowing about color. Neuropsychologia. 2007; 45:2802–10. [PubMed: 17575989]

Talairach, J.; Tournoux, P. Co-planar Stereotaxic Atlas of the Human Brain: 3-Dimensional Proportional System - an Approach to Cerebral Imaging. Thieme Medical Publishers; New York: 1988.

Tsapkini K, Rapp B. The orthography-specific functions of the left fusiform gyrus: Evidence of modality and category specificity. Cortex. 2010; 46:185–205. [PubMed: 19428003]

van Essen DC, Maunsell JHR. Two-dimensional maps of the cerebral cortex. J Comp Neurol. 1980; 191:255–81. [PubMed: 7410593]

Vidorreta JG, Garcia R, Moritz-Gasser S, Duffau H. Double dissociation between syntactic gender and picture naming processing: A brain stimulation mapping study. Hum Brain Mapp. 2011; 32:331–40. [PubMed: 21319264]

Vogt C, Vogt O. Allgemeinere Ergebnisse unserer Hirnforschung. J Psychol Neurol. 1919; 25:279–461.

von Economo, C. The cytoarchitectonics of the human cerebral cortex. Oxford University Press; London: 1929.

West M, Slmianka L, Gundersen H. Unbiased Stereological Estimation of the Total Number of Neurons in the Subdivisions of the Rat Hippocampus Using the Optical Fractionator. Anat Rec. 1991; 231:482–97. [PubMed: 1793176]

Wierenga C, Perlstein W, Benjamin M, Leonard C, Rothi L, Conway T, Cato M, Gopinath K, Briggs R, Crosson B. Neural substrates of object identification: Functional magnetic resonance imaging evidence that category and visual attribute contribute to semantic knowledge. J Int Neuropsychol Soc. 2009; 15:169–81. [PubMed: 19232155]

Highlights

We tested a combined mri-microscopy protocol applied to the same subject.

We used mri-based automated segmentation to define the region of interest.

We used a large-scale stereological approach on whole-brain histological slices

The results show it is possible to link histological data directly to mri mapping.

Method may help clarify structure-function relationships in human cerebral cortex.
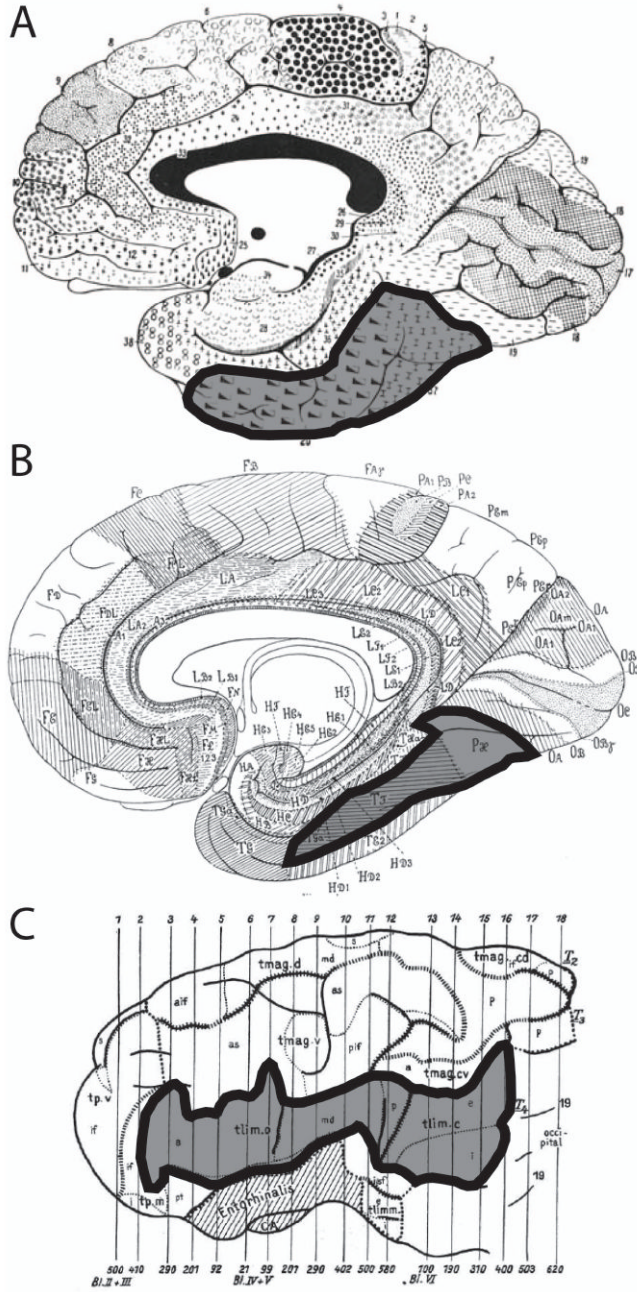
Figure 1.
Classical cortical architectonic maps based on A. density and thickness of cellular layers (Brodmann, 1909); B. density and thickness of cellular layers, as well as estimates of cell size and density (von Economo, 1929); C. the arrangement and orientation of intracortical fibers (Hopf, 1951). The region corresponding to the FG is highlighted on each map.
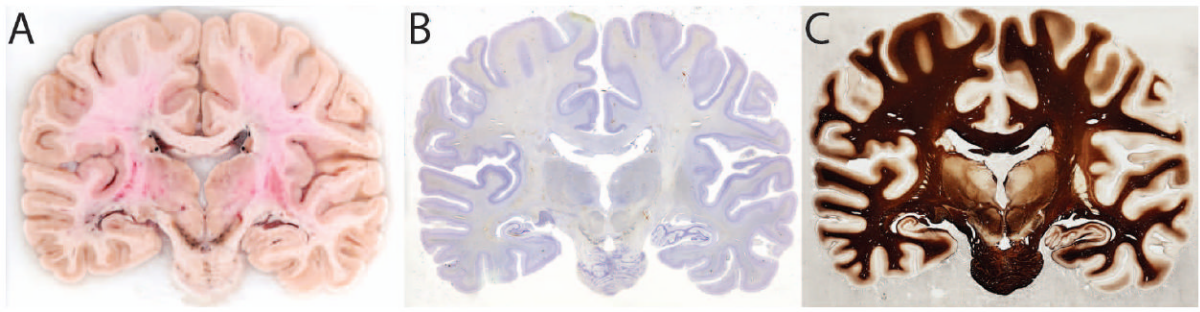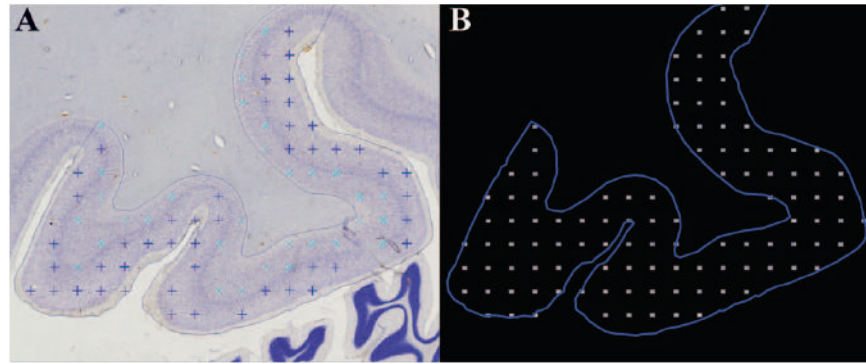
Figure 2.
Images of a coronal section through the specimen. A. Blockface image acquired with a Nikon D700 camera (original resolution of 45μm/pixel) immediately before the tissue section was collected; B. The section corresponding to the blockface image, mounted on a large-format (5×7in) glass slide and stained for Nissl substance (Simmons and Swanson, 1993), which allows for the visualization of cell bodies; C. The section adjacent to the blockface image, mounted and stained using a modified Gallyas silver impregnation stain (Gallyas, 1979), which allows for the visualization of myelinated connections between neurons.
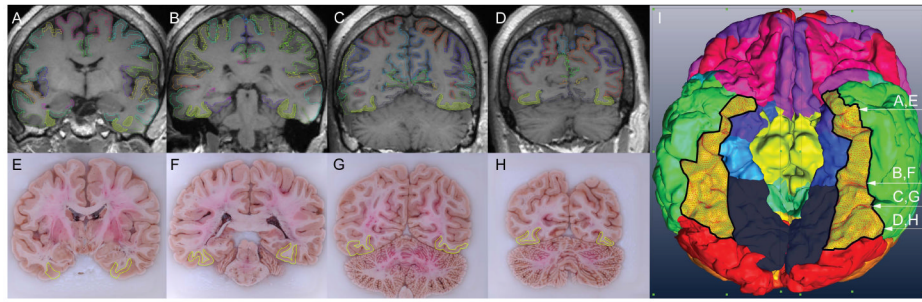
Figure 3.
Images of the process of automated parcellation of the MRI of the brain specimen using FreeSurfer (Fischl, 2012) yielding the region of interest. A-D. Coronal sections through the MRI. Hatched region indicates the FG; E-H. Blockface images corresponding to A-D, with the FG outlined. I. The surface of the brain as reconstructed and segmented using the MRI and FreeSurfer. The FG is outlined in black. Arrows indicate the approximate positions of the coronal sections in relation to the surface reconstruction.
Scan parameters: 3-D acquisition, T1-weighted, fast gradient echo; pixel spacing: 0.9375mm × 0.9375mm; slice thickness: 1.2mm; TE=4.832; TR=10.612.

Figure 4.
Illustration of the data acquisition in Stereo Investigator. A. Image of the Nissl-stained FG with markers indicating counted neurons; B. The outline of the sampled ROI and the grid of acquired image stacks in which neurons were counted.
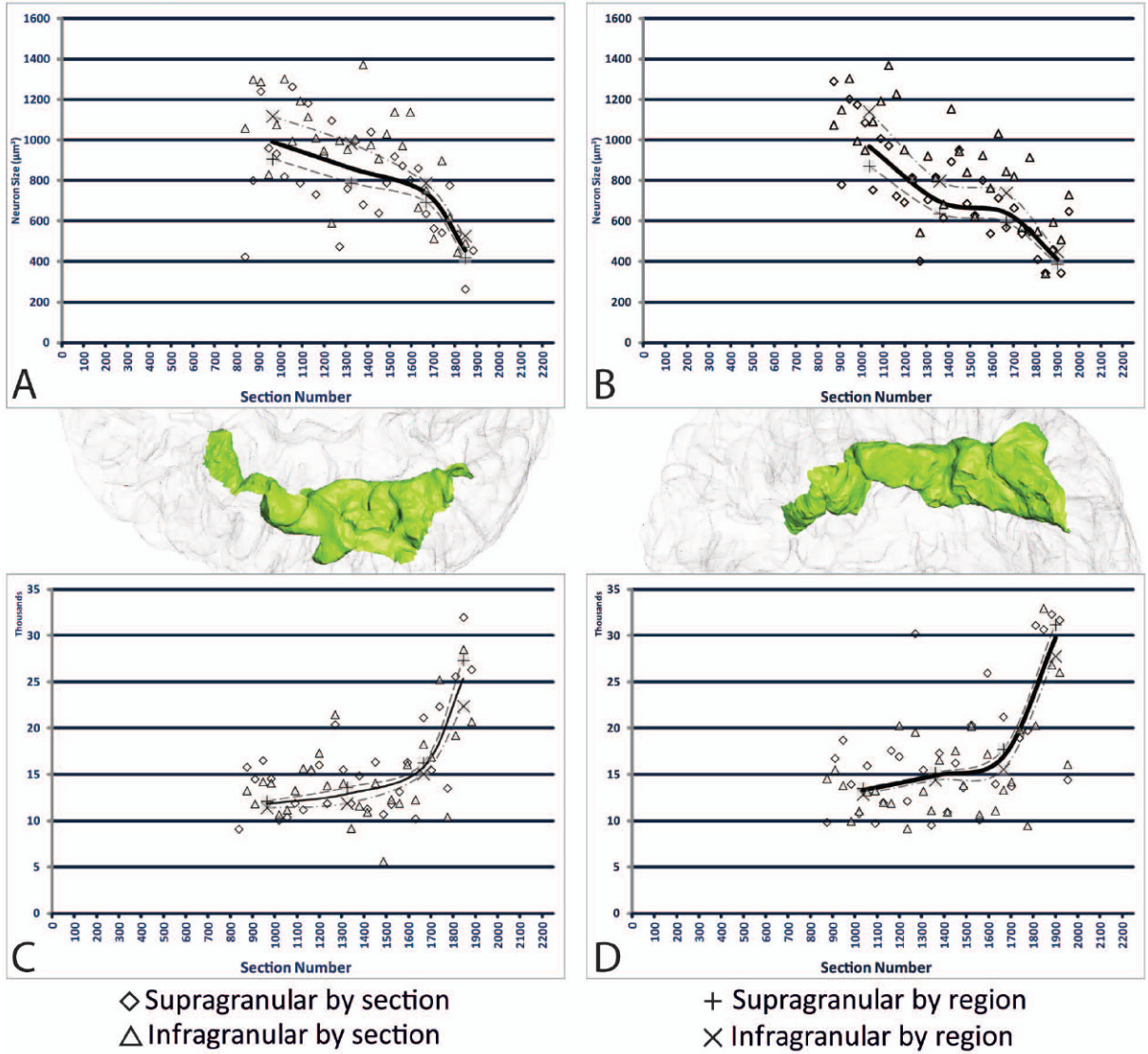
Figure 5.
The stereological data in the right and left FG for neuron size and neuron density plotted against section number (actual section collected). A. Neuron size in right FG; B. Neuron size in left FG; C. Neuron density in right FG; D. Neuron density in left FG. The X (supragranular) and + (infragranular) indicate the values for each sub region, while the solid line is the average across regions for both supra-and infra- granular regions together. Neuron size and neuron density vary inversely with each other. Posterior regions exhibit greater neuron density with smaller neuron size, while anterior regions display larger neuron size with lesser neuron density.
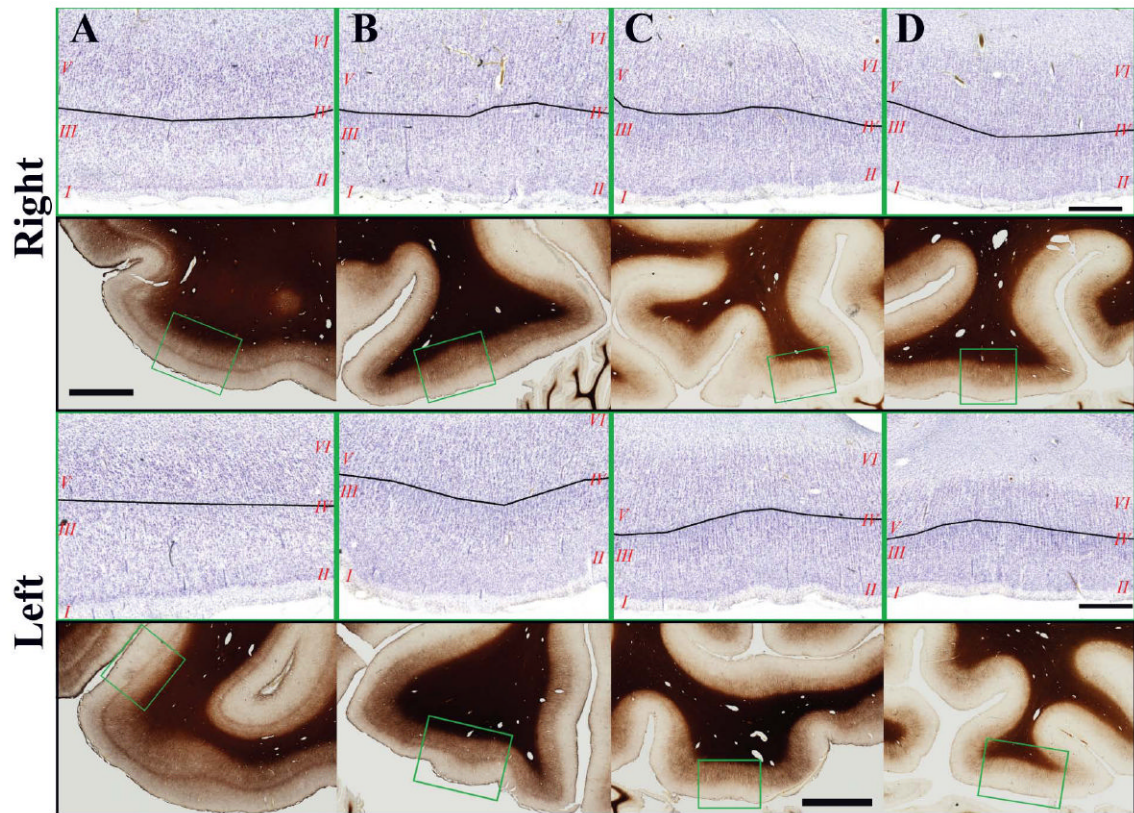
Figure 6.
A-D. Photomicrographs of the Nissl-stained cortex (with cortical layers numbered in red, and black lines indicating the approximate location of the boundary between supragranular and infragranular layers) and the adjacent sections stained for myelination (green box indicates the location of the Nissl-stained image) in the Right (top) and Left (bottom) FG. These images correspond to the sections illustrated in Figure 3. Scale bars: Nissl 100μm; Myelin 500mm.

Table I

Estimated volume (mm^3) of the FG and its sub regions. Regions A-D refer to the 4 sub-regions identified via analysis of myelination.

	Right	Left
Region A	1301	1905
Region B	3962	2653
Region C	2330	2816
Region D	660	564
Total	8252	7930

Table II

Stereological estimations of neuronal number and cell size. Regions A–D refer to the 4 sub-regions identified via analysis of myelination.

A. Right	Infragranular			Supragranular		
	Number (×10⁶)	Density (#/mm³)	Size (μm³)	Number (×10⁶)	Density (#/mm³)	Size (μm³)
Region A	6.7*	11411	1118.2	8.9	12120	906.9
Region B	20.1	11894	984.6	31.0	13603	788.0
Region C	15.3	15082	788.1	21.7	16257	693.9
Region D	6.2*	22396	527.1	11.0*	27346	419.7
Average	50.4	14126	859.3	75.6	15896	706.6

B. Left	Infragranular			Supragranular		
	Number (×10⁶)	Density (#/mm³)	Size (μm³)	Number (×10⁶)	Density (#/mm³)	Size (μm³)
Region A	10.1	12871	1140.8	15.8	13521	871.5
Region B	15.3	14407	798.4	24.0	15165	637.8
Region C	17.2	15580	740.0	30.5	17724	594.5
Region D	6.6*	27788	448.9	10.2*	31208	388.0
Average	49.3	15382	778	80.5	16702	619.4

*
C.E. (Gundersen, m=1) greater than 0.05.

Table III

Asymmetry in quantitative estimations. Regions A–D refer to the 4 sub-regions identified via analysis of myelination.

	Volume	Number		Density		Size	
		Infra	Supra	Infra	Supra	Infra	Supra
Region A	-0.38 *	-0.40 *	-0.56 *	-0.12 *	-0.11 *	-0.02	0.04
Region B	0.40 °	0.27 °	0.25 °	-0.19 *	-0.11 *	0.21 °	0.21 °
Region C	-0.19 *	-0.12 *	-0.34 *	-0.03	-0.09 *	0.06 °	0.15 °
Region D	0.16 °	-0.06 *	0.08 °	-0.21 *	-0.13 *	0.16 °	0.08 °
Average	0.04	0.02	-0.06 *	-0.09 *	-0.05	0.10 °	0.13 °

*
Left greater than right asymmetry of 5% or more

°
Right greater left asymmetry of 5% or more